Journal of Power Sources 203 (2012) 145–152

Contents lists available at SciVerse ScienceDirect

Journal of Power Sources

journal homepage: www.elsevier.com/locate/jpowsour

The effect of rare earth metals on the microstructure and electrochemical corrosion behavior of lead calcium grid alloys in sulfuric acid solution

Wenqing Zhang[a,d,e], Aiju Li[a,b,*], Hongyu Chen[d,e,**], Bingyan Lan[a], Ke Pan[a], Tianren Zhang[b], Mingxue Fang[b], Sanyuan Liu[b], Wei Zhang[c]

[a] School of Chemistry and Environment, South China Normal University, Guangzhou, Guangdong 510006, China
[b] Zhejiang Tianneng Battery Co. Ltd., Huzhou, Zhejiang 313117, China
[c] Zhuzhou Smelter Group Co. Ltd., Zhuzhou, Hunan 412004, China
[d] Base of Production, Education & Research on Energy Storage and Power Battery of Guangdong Higher Education Institutes, Guangzhou, Guangdong 510006, China
[e] Engineering Research Center of Materials and Technology for Electrochemical Energy Storage of Ministry of Education, Guangzhou, Guangdong 510006, China

ARTICLE INFO

Article history:
Received 6 August 2011
Received in revised form
22 November 2011
Accepted 24 November 2011
Available online 3 December 2011

Keywords:
Rare earth metals
Lead–calcium grid alloys
Anodic film
Corrosion resistance

ABSTRACT

The effect of the rare earth element lanthanum (La) on the microstructure of lead–calcium grid alloys was studied by the metallographic microscope. A comparison of the electrochemical corrosion behavior of the new and traditional grid alloys was investigated by cyclic voltammetry (CV), A.C. impedance and electrochemical impedance spectroscopy (EIS). Scanning electron microscopy (SEM) and X-ray photoelectron spectroscopy (XPS) were used to study the surface morphology of anodic films of Pb–Ca–Sn–Al–Re alloys formed in sulfuric acid solution at 1.3 and 0.9 V for 2 h. The morphology of the corrosion layer was analyzed by SEM after the constant current corrosion test. The results show that an appropriate content of La can effectively (1) increase the fineness of the grain of Pb–Ca–Sn–Al alloys, (2) increase the growth of PbO_2 film, and (3) make the anodic film formed at 1.3 V become fine and compact. Alloys with contents of 0.01 wt.%, 0.03 wt.% and 0.1 wt.% La were shown satisfactory results. La also can decrease the growth of Pb(II) film, purify and increase the density of the anodic film at 0.9 V, especially for La content of 0.03 wt.% and 0.1 wt.%. Moreover, La can improve the corrosion resistance of Pb–Ca–Sn–Al alloys, particularly for a La content of 0.01 wt.%.

© 2011 Elsevier B.V. All rights reserved.

1. Introduction

Lead–calcium alloys are widely used for the positive grid materials of valve-regulated lead-acid (VRLA) batteries because of their high hydrogen overpotential, low self-discharge characteristics, and ability to meet the maintenance-free requirements of batteries. However, the Pb–Ca alloys cause premature capacity loss (PCL) [1,2] of batteries due to the formation of a passive, high-resistivity layer on the surface of the Pb–Ca alloys. Moreover, the creep resistance of Pb–Ca alloys is inferior, causing growth of the grid. To improve the performances of lead–calcium grid alloys, many researchers dedicated to add rare earth metals. Preliminary results indicated improvements of lead–calcium grid alloys, including the mechanical properties, corrosion resistance and conductivity of grids used in lead-acid batteries.

Rare earth elements possessed an atomic radius close to that of lead are becoming increasingly important in battery chemistry. Rare earth elements can easily be absorbed, and deposit on the surface of grain boundaries during alloy solidification, sequentially forming a film, which can inhibit the growth of the grains and refine the grains. Moreover, this film can decrease the impedance of the anodic film, as well as increase the corrosion resistance of the grid alloys.

During the past few years, many studies have focused on finding a suitable additive to improve the performance of lead and lead alloys, e.g. Sn, Bi, Sr, Cd and Ag [3–5]. Rare earth elements are extensively used in the metallurgy industry to improve the fine grain structure of alloys in order to enhance their corrosion and abrasion resistance. Several authors studied lead–calcium and lead-antimony alloys that contained rare earth metals. Yang et al. [6] found that rare earth elements improved the hydrogen overpotential and corrosion resistance of Pb–Sb alloys. Lin et al. [7] concluded that the addition of cerium can restrain the hydrogen and oxygen evolution of Pb–Ca–Sn alloys. Li et al. [8] demonstrated that lanthanum can decrease the oxygen evolution, restrain the growth

* Corresponding author at: School of Chemistry and Environment, South China Normal University, Guangzhou 510006, China. Tel.: +86 20 39310212; fax: +86 20 39310212.
** Corresponding author at: Base of Production, Education & Research on Energy Storage and Power Battery of Guangdong Higher Education Institutes, Guangzhou, Guangdong 510006, China. Tel.: +86 20 39310183; fax: +86 20 39310183.
E-mail addresses: liaiju@scnu.edu.cn (A. Li), battery@scnu.edu.cn (H. Chen).

0378-7753/$ – see front matter © 2011 Elsevier B.V. All rights reserved.
doi:10.1016/j.jpowsour.2011.11.067

Table 1
The lanthanum content in the Pb–Ca–Sn–Al–La alloys.

Alloy	1#	2#	3#	4#	5#	6#
La (wt.%)	0	0.005	0.01	0.03	0.05	0.1

of Pb(II) and PbO_2, decrease the resistance of the anodic film, and improve the corrosion resistance of Pb alloys.

In this paper, the effect of the rare earth element La on the microstructure of lead–calcium grid alloys was studied by the metallographic microscope. A comparison of the electrochemical corrosion behavior of the new and traditional grid alloys was investigated by cyclic voltammetry (CV), A.C. impedance and electrochemical impedance spectroscopy (EIS). Scanning electron microscopy (SEM) and X-ray photoelectron spectroscopy (XPS) were used to study the surface morphology of anodic films of Pb–Ca–Sn–Al–Re alloys formed in sulfuric acid solution, and the morphology of the corrosion layer was analyzed by SEM after a constant current corrosion test.

2. Experimental

Pb–Ca–Sn–Al–La alloys were processed by melting mixtures of pure: lead (99.994%); calcium (99.75%); tin (99.99%); aluminum (99.7%); and lanthanum (99.95%) in an electrical furnace under an argon gas atmosphere at 800 °C for 15 min. After cooling down to room temperature, they were formed into rods with a 0.4 cm^2 end face to serve as the working electrodes. The content of La in the Pb–Ca–Sn–Al–La alloys is listed in Table 1.

The metallographic samples were prepared from the alloy rods. These samples were then chemically polished using a 1:1 (by volume) acetic acid/hydrogen peroxide solution, and etched with a solution containing 9 g ammonium molybdate, and 15 g citric acid in 90 g double-distilled water. The metallographic microstructure of each example was observed with a Nikon LV-UEPT polarizing microscope.

Electrochemical tests were performed in a three-electrode configuration using an Autolab PGSTAT-30 potentionstat/galvanostat (ECO Echemie B.V., Holland). The counter and reference electrodes were a platinum plate (0.3 cm^2) and Hg/Hg_2SO_4 electrode (1.28 g cm^{-3} H_2SO_4 solution, E = +0.658 vs. SHE), respectively. All potentials reported here are relative to the reference electrode. The electrolyte was 1.28 g cm^{-3} sulfuric acid solution, which was prepared from analytical grade reagent and maintained at 25 °C. Prior to each experiment, all working electrodes were first mechanically polished successively by 600#, 1000# and 2000# SiC emery papers, then washed by double-distilled water. The polished electrode was reduced at −1.2 V to eliminate oxides on the electrode surface.

Corrosion tests were conducted in cells assembled in series, using Pb–Ca–Sn–Al alloys with different amounts of La as the positive electrode and Pb as the negative electrode. The corrosion test was carried out with a constant current of 10 mA cm^{-2} at room temperature for 30 days. The corrosion layer of one corroded electrode for each alloy was removed using a boiling solution containing 4 g glucose and 20 g sodium hydroxide in 200 g double-distilled water. The corrosion layer was retained on the surface of the other corroded electrode, and the morphology of the corrosion layers and corroded surfaces of the Pb–Ca–Sn–Al alloy electrodes with different amounts of La was analyzed using a JSM-6380 scanning electron microscope (SEM), after washing and drying.

Surface analysis by X-ray photoelectron spectroscopy (XPS) was carried out with a VGA Scientific MK II(ESCALAB 250) apparatus, using an Al Kα X-ray source. The X-ray power was 150 W, Pb_{4f} binding energies were determined with a C_{1s} (284.80 eV) reference.

3. Results and discussion

3.1. Metallographic microstructure

Fig. 1 presents the metallographic microstructure of Pb–Ca–Sn–Al alloys with different La contents: the 1# alloy has a massive coarse crystal structure with anomalous grain boundaries; the grains of 2# and 5# alloys are smaller than 1#, but the grain boundaries are smooth and clear, and the grain of 2# alloy is very regular; with the increase of La content, the 3#, 4# and 6# alloys show similar structure with fine grains and regular boundaries, which can protect the lead alloys from being recrystallized, and hence improve the stability of the structure compared with that of 1#. Additionally, the fine grain microstructure shape can consume more energy formed during the tenacity transformation, and then improve the tenacity behavior of the alloys [9].

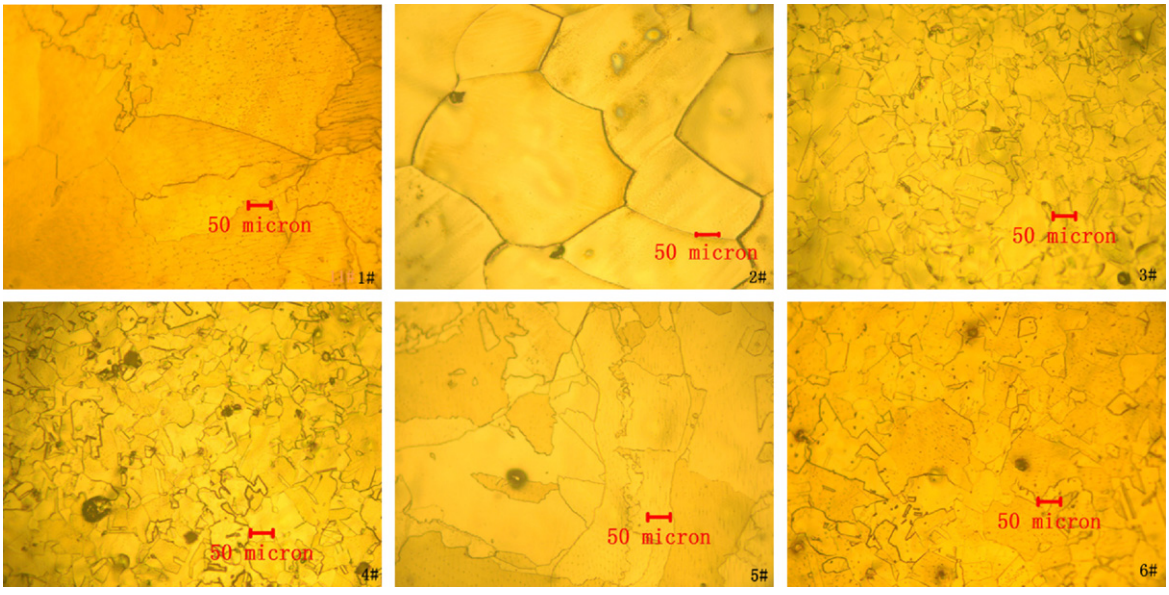

Fig. 1. Metallographic microstructure of Pb–Ca–Sn–Al alloys with different La contents (200×).

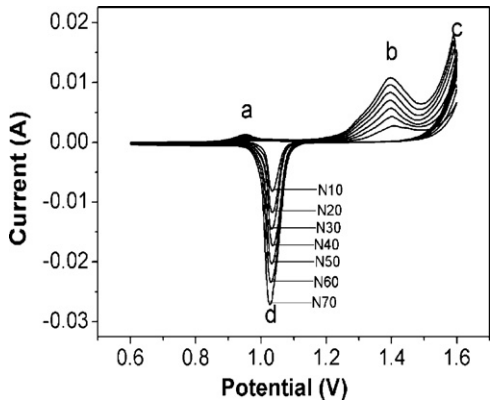

Fig. 2. Cyclic voltammograms for a Pb–Ca–Sn–Al electrode (1#) in 1.28 g cm^{-3} H_2SO_4 for the 10th, 20th, 30th, 40th, 50th, 60th and 70th cycle (scan rate = 5 mV s^{-1}).

3.2. Cyclic voltammetry

Fig. 2 illustrates the cyclic voltammograms for 1# electrode in 1.28 g cm^{-3} H_2SO_4 for the 10th, 20th, 30th, 40th, 50th, 60th and 70th cycle performed between 0.6 V and 1.6 V at a sweep rate of 5 mV s^{-1}, the cyclic voltammograms of other electrodes are not shown since they have similar shapes to those in Fig. 2. It can be seen that three anodic peaks (a), (b) and (c) appear in the positive sweeping, which correspond to: the oxidation of the alloy substrate to α-PbO_2; the transformation of $PbSO_4$ to β-PbO_2; and the evolution of oxygen, respectively; and peak (d) observed in the negative sweeping corresponds to the reduction of PbO_2 to $PbSO_4$.

Fig. 3 shows the reduction cycle charges of the peak d (PbO_2/$PbSO_4$) (Qred) for Pb–Ca–Sn–Al alloy electrodes with different La contents at the 10th, 20th, 30th, 40th, 50th, 60th and 70th cycle in the cyclic voltammograms, the slop ration reflects the growth of cathodic reduction charges. From Fig. 3, it can be seen that there is a good linear relationship between cathodic reduction charges (Qred) and the cycles (N), and when the La content is lower than 0.03 wt.%, the growth of cathodic reduction charges of 2# electrodes is obviously lower than 1# electrode, 3# is close to that of 1#, the growth rate of 2# is the least; while the La content is 0.03 wt.% or more, the growth of cathodic reduction charges of 4# and 6# electrodes are higher than 1# electrode, except 5#. This suggests that there was less PbO_2 formed on 2#, 3# and 5# alloy electrodes while more PbO_2 formed on 4# and 6# alloy electrodes. It indicates that when the La content is 0.005 wt.%, 0.01 wt.% and 0.05 wt.%, which facilitates to decrease the growth

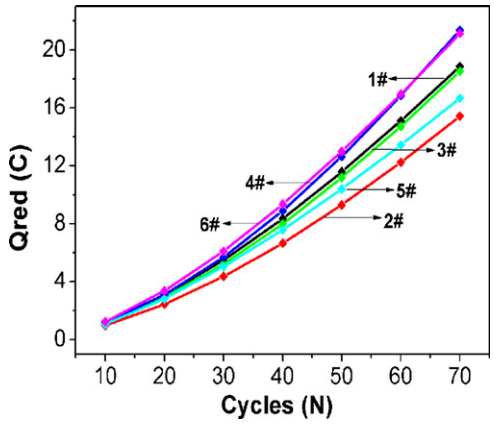

Fig. 3. Reduction cycle charges of the peak d (PbO_2/$PbSO_4$) (Qred) for Pb–Ca–Sn–Al alloy electrodes with different La contents at the 10th, 20th, 30th, 40th, 50th, 60th and 70th cycle.

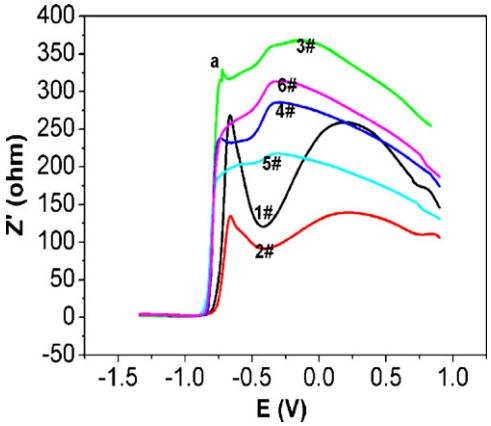

Fig. 4. Z′ vs. *E* plots of the anodic films formed on Pb–Ca–Sn–Al alloy electrodes with different La contents at 0.9 V in 1.28 g cm^{-3} H_2SO_4 solution for 1 h (scan rate = 1 mV s^{-1}, *f* = 1 000 Hz).

rate of the anodic corrosion PbO_2 layer, consequently increase the corrosion resistance of the Pb–Ca–Sn–Al alloy, especially the 2# (0.005 wt.% La) alloy. Though the additive of La intends to increase the growth rate of the anodic PbO_2 film when the La content is 0.03 wt.% and 0.1 wt.%. La possibly changed the microstructure of the alloys and the morphology of $PbSO_4$ crystals [10].

3.3. A.C. voltammetry

The high resistivity characteristic of the anodic film mainly depends on the composition of Pb(II) film formed on lead alloys, and the resistivity of the PbO crystal is high to 10^{11} Ω cm^{-2}, which easily causes to the premature capacity loss. The variation of the impedance of the anodic film with a negative linear potential sweep had been measured by A.C. voltammetry.

Fig. 4 provides the plots of Z′ (real part of the impedance) vs. potential (E) of the anodic films formed on Pb–Ca–Sn–Al alloy electrodes with different La contents at 0.9 V in 1.28 g cm^{-3} H_2SO_4 solution for 1 h. It can be observed that the Z′ remains at a high level until about −0.75 V, and produces a peak at −0.66 to −0.75 V, then drops dramatically to a low level, which correspond to the change from PbO_n ($1 < n < 2$) to PbO, highly resistive Pb(II) oxide film to electrically conductive Pb metal [11], respectively. Fig. 5 evidences the relationship between Z′ of peak a (at −0.66 to −0.75 V) and La weight. It is compared from Fig. 5 that the resistance of the anodic films of 2#, 4#, 5# and 6# electrodes is lower than that on 1# electrode except the 3# alloy. It suggests that the addition of La may

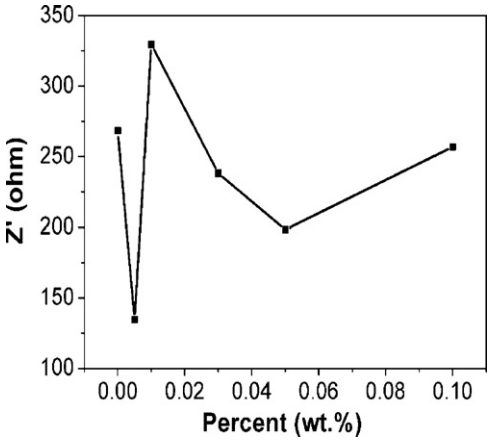

Fig. 5. Relationship between Z′ of peak a (−0.66 to −0.75 V) and La weight.

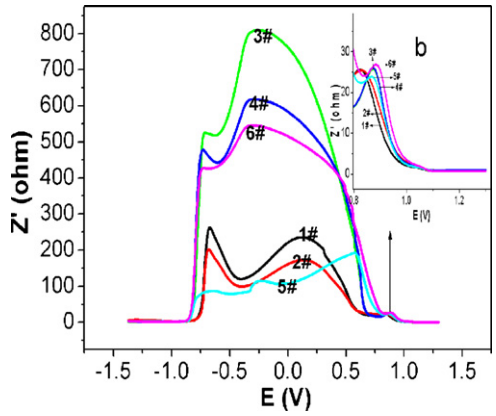

Fig. 6. Z vs. E plots of the anodic films formed on Pb–Ca–Sn–Al alloy electrodes with different La contents at 1.3 V in 1.28 g cm^{-3} H_2SO_4 solution for 1 h (scan rate = 1 mV s^{-1}, f = 1000 Hz).

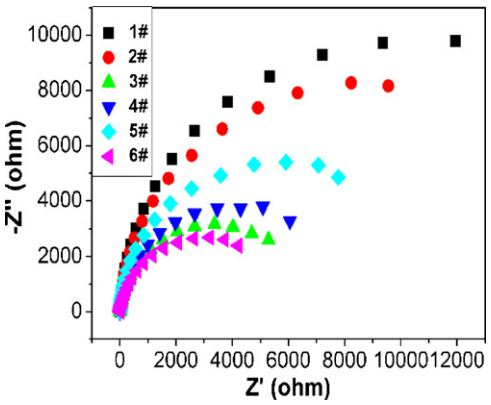

Fig. 7. Nyquist plots of Pb–Ca–Sn–Al alloy electrodes with different La contents at 1.3 V for 2 h in 1.28 g cm^{-3} H_2SO_4.

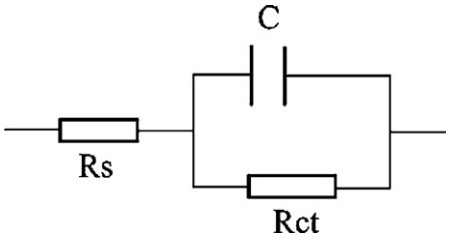

Fig. 8. The electrical equivalent circuit for Fig. 7.

inhibit the growth of anodic Pb(II) film, reduce the resistance of the anodic Pb(II) film, as well as increase the conductivity of anodic films formed on Pb–Ca–Sn–Al alloys. And 2# alloy with 0.005 wt.% La was found to have the most optimum addition.

Fig. 6 shows the Z′ (real part of the impedance) vs. E plots of the anodic films formed on Pb–Ca–Sn–Al alloy electrods with different amounts of La at 1.3 V in 1.28 g cm^{-3} H_2SO_4 solution for 1 h. Fig. 6(b) is the amplifier of Fig. 6 from 0.5 V to 1.3 V. The main component of the anodic films of lead alloys formed at 1.3 V are PbO_2, $PbSO_4$ and Pb(II). Since the resistivity of the PbO_2 crystal is quite low (at about 10^{-3} Ω cm) compared to other lead oxides in the anodic film, the value of Z′ is rather small in the initial stage of the potential sweeping to negative direction (1.3–1.0 V) in Fig. 6(b). It can be seen that PbO_2 has not been reduced in the initial stage of electric potential scan (1.3–1.0 V). When the potential goes up to 1.1 V, the Z′ of the alloy electrodes all begin to increase and reaches maximum at 0.9 V ~0.825 V, which corresponds to the reduction of α-PbO_2 to PbO_{1+x} ($0 < x < 1$). Then the oxidation of a little amount of Pb(II) to α-PbO_2 occurs and causes the decrease of the Z′ slightly. It can be found from Fig. 6(b) that change of Z′ for 2#, 3#, 4# and 6# alloy electrodes are almost larger than that for 1# alloy electrode except 5# from 0.9 V to 0.825 V, and it also means that there are more PbO_2 film formed on Pb–Ca–Sn–Al–La alloy electrodes than that on Pb–Ca–Sn–Al alloy electrode. So it can be concluded that La can increase the growth of the anodic PbO_2 film, thus improving the conductivity of the anodic film formed on Pb–Ca–Sn–Al alloys.

3.4. The micrograph and composition study of anodic film formed at 1.3 V

3.4.1. EIS

The EIS is a powerful, nondestructive, and informative technique, which is usually used for characterization and study of corrosion phenomena [12], fuel cells and batteries [13], coatings

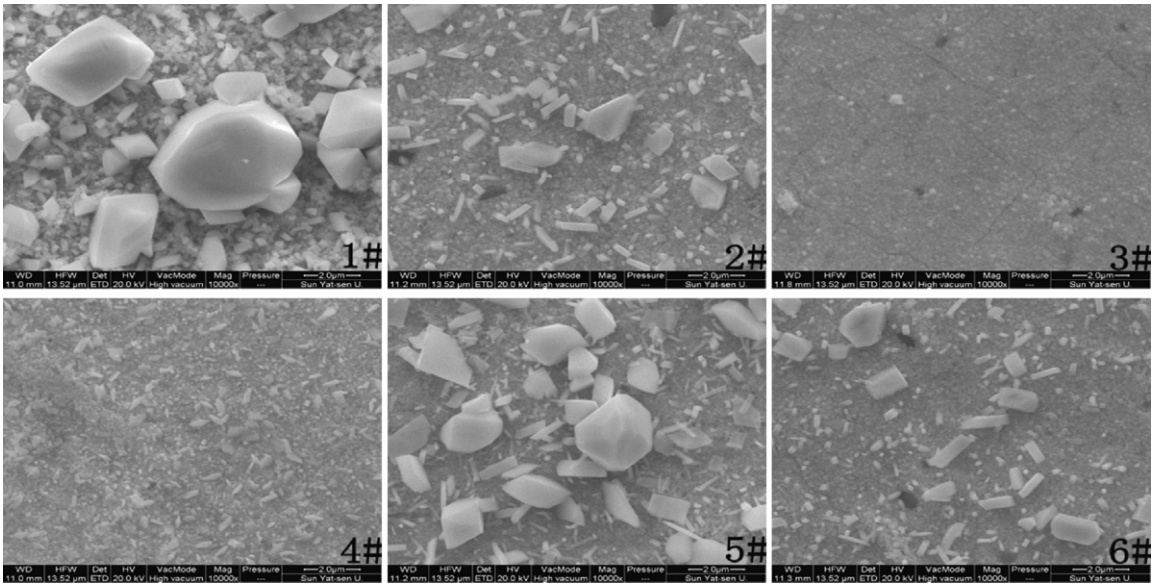

Fig. 9. SEM analysis of anodic films formed on Pb–Ca–Sn–Al alloys with different La contents after EIS measure at 1.3 V oxidized for 2 h in 1.28 g cm^{-3} sulfuric acid solution (10,000×).

Table 2
Resistance of anodic films formed on Pb–Ca–Sn–Al alloy electrodes with different La contents at 1.3 V for 2 h in 1.28 g cm^{-3} H_2SO_4.

Alloy	R_s (Ω)	R_{ct} (kΩ)	C (mF)	n
1#	8.17	19.78	0.6483	0.9880
2#	6.86	17.07	0.6583	0.9780
3#	7.44	6.76	1.085	0.9591
4#	7.13	7.86	1.052	0.9771
5#	6.60	11.51	0.788	0.9598
6#	6.69	6.09	1.297	0.9261

Table 3
Comparison of banding energies for compounds with standard data.

Items	Compounds	Pb_{4f} (eV)	S_{2p} (eV)	O_{1s} (eV)
Standard data	PbO_2	137.4		531.00
	PbO	138.9		531.90
	$PbSO_4$	139.4	168.60	531.20
Experimental data	2# (0.005 wt.% La)	139.340	168.557	532.157
		138.071	163.375	531.292
		136.629		530.353

and conductive polymers [14], adsorption behavior of thin films [15–17], and electron transfer kinetics [18]. This method was used to study the anodic charge transfer resistance of Pb–Ca–Sn–Al–La new grid alloys prepared in this work.

1.3 V is the growth potential for PbO_2 on the positive grid alloys when the battery is undergoing a float charge. PbO_2 is the major product of anodic corrosion, so the amount of PbO_2 can be used to evaluate the extent of corrosion of the positive grid alloy. Therefore, the electrochemical experiments focused upon the formation of PbO_2 on Pb–Ca–Sn–Al alloys with different La contents in sulfuric acid solution.

Fig. 7 is Nyquist plots of Pb–Ca–Sn–Al alloy electrodes with different La contents in 1.28 g cm^{-3} H_2SO_4 at 1.3 V for 2 h. It reveals that the electrochemical impedance plot of the 2#, 3#, 4#, 5# and 6# alloy electrodes is similar to that of the 1# electrode. The plots show a semicircular region at high frequency, which are associated with an electron-transfer step. Consequently, the electrochemical impedance behavior shown in Fig. 7 can be represented by a simple equivalent circuit (Fig. 8). The fitting results are listed in Table 2. R_s denotes solution resistance, R_{ct} and C indicate the resistor of the anodic film and capacity of the electric double-layer, respectively.

The results show that solution resistance (R_s) of the 2#, 3#, 4#, 5# and 6# alloy is lower than that of 1# alloy. When adding La into the Pb–Ca–Sn–Al alloys, the Pb(II) content (PbO or $PbSO_4$) decreases significantly, that is, the La can restrain the development of the Pb(II), and improve the conductivity of the interface between grid

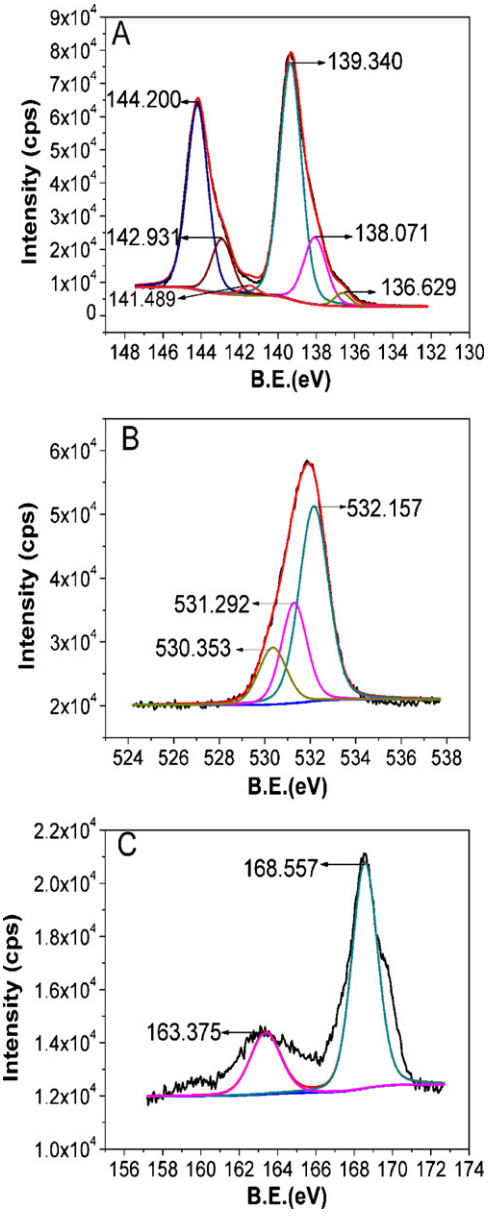

Fig. 11. XPS separation spectrum of Pb_{4f}, O_{1S} and S_{2P} element of 2# alloy (0.005 wt.% La) after EIS measure at 1.3 V oxidized for 2 h in 1.28 g cm^{-3} sulfuric acid solution (A: Pb_{4f}; B: O_{1S}; C: S_{2p}).

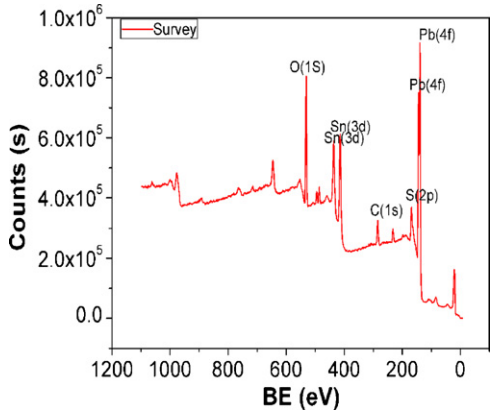

Fig. 10. Survey spectra of all anodic scales of 2# alloy (0.005 wt.% La) after EIS measure at 1.3 V oxidized for 2 h in 1.28 g cm^{-3} sulfuric acid solution.

matrix and active material, then can reduce the premature capacity loss of the battery.

From Table 2, it can apparently find that the impedance values of the anodic film of 2#, 3#, 4#, 5# and 6# alloy electrodes are lower than that of 1# electrode, and those of 3#, 4# and 6# are close and relatively lower than 2# and 5#. This indicates that the 2#, 3#, 4#, 5# and 6# alloys may increase the growth of the PbO_2, and then improve the conductivity of passive films formed on Pb–Ca–Sn–Al alloys.

It is indicated in Table 2 that capacitance values of 2#, 3#, 4#, 5# and 6# alloys all are higher than that of 1# alloy, but those of 3#, 4# and 6# are very close, while 1#, 2# and 5# are also very close. La can also decrease the thickness of the anodic layer and promote the compactness of the corrosion layer, and increase the quantities of the cavities and electrons, then enhance the conductivity of the corrosion layer. All these characteristics are helpful to the deep recycling property of the battery.

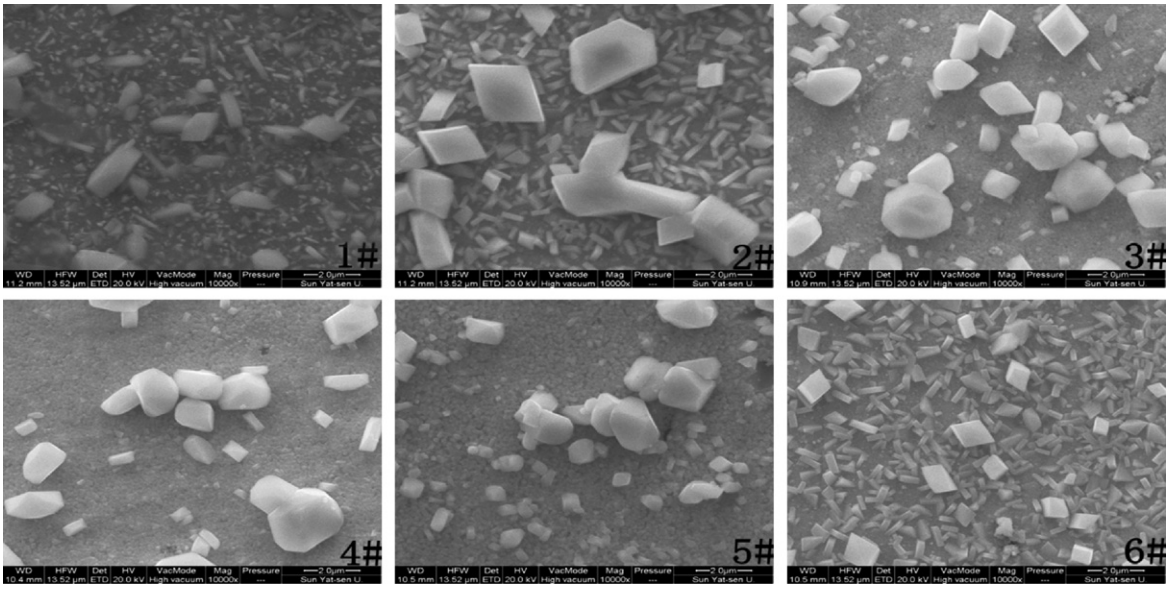

Fig. 12. SEM analysis of anodic films formed on Pb–Ca–Sn–Al alloy electrodes with different La contents after EIS measure at 0.9 V oxidized for 2 h in 1.28 g cm^{-3} sulfuric acid solution (10,000×).

3.4.2. SEM

Scanning electron micrographs of the surface of the anodic films formed on Pb–Ca–Sn–Al alloy electrodes with different La contents after electrochemical impedance spectroscopy (EIS) measure at 1.3 V oxidized for 2 h are shown in Fig. 9.

Scanning electron micrographs show that the morphology of the anodic film is affected by the addition of La. The structure of anodic film formed on 1# and 5# alloys is loose and the size is large, but the structure of the anodic film formed on 2#, 3#, 4# and 6# alloys appears compact and small. This reveals that addition of La can refine the size and increase the density of anodic film formed at 1.3 V, then improve the corrosion resistance of Pb–Ca–Sn–Al alloy. The addition of 0.01 wt.% La (3# alloy) was found to be the most effective one.

3.4.3. X-ray photoelectron spectroscopy (XPS)

Fig. 10 is the survey spectra of all the anodic scales of 2# after electrochemical impedance spectroscopy (EIS) measure at 1.3 V oxidized for 2 h. Peaks of Pb_{4f}, O_{1s}, C_{1s} and Sn_{3d} in the alloy scale are apparent. Fig. 11 and Table 3 show that the anodic scales of 2# alloy mainly consists of PbO_{1+x} (PbO_2 and PbO) and $PbSO_4$, which has better conductivity and good mechanical behavior than Pb(II) and is helpful to improve the deep recycling property of the battery. While it is reported that the anodic scales of traditional Pb–Ca alloys is mainly composed of Pb(II) ($PbSO_4$ and PbO) [19]. It seems that the rare earth element La can restrain the development of the Pb(II) and encourage the development of Pb(IV) in the anodic film.

3.5. The micrograph study of anodic film formed at 0.9 V

0.9 V is the growth potential for PbO on the positive grid alloys when the battery is undergoing a deep-discharge. Fig. 12 presents the structure of anodic films formed on Pb–Ca–Sn–Al alloys with different La contents after electrochemical impedance spectroscopy (EIS) measure at 0.9 V oxidized for 2 h in 1.28 g cm^{-3} sulfuric acid solution. It is found that the anodic films formed on

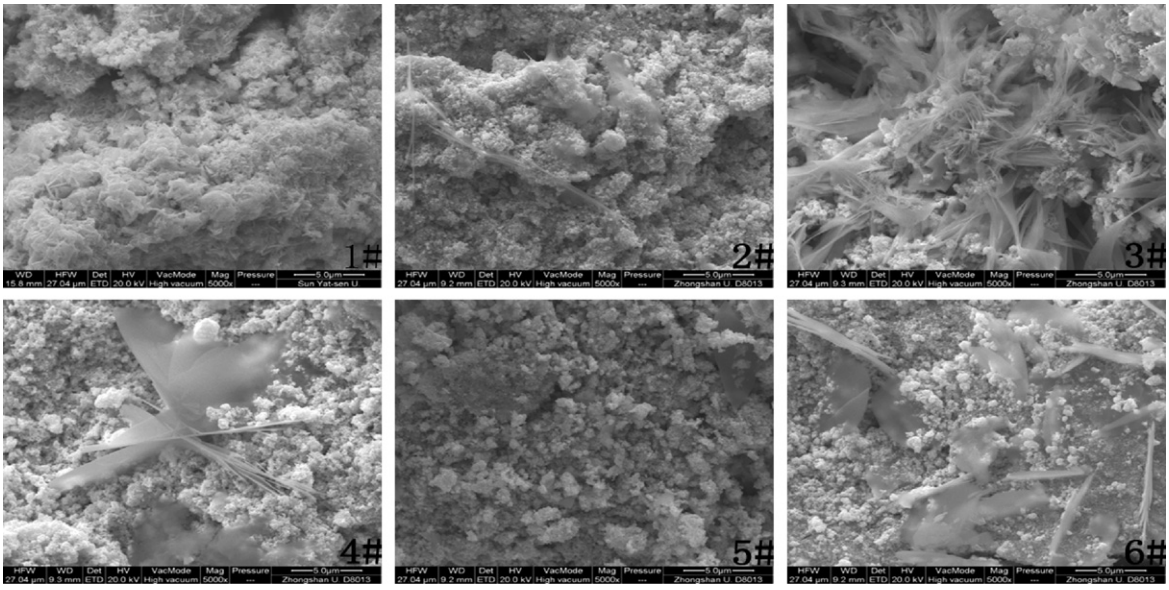

Fig. 13. Morphology of the corrosion layers formed on Pb–Ca–Sn–Al alloy electrodes with different La contents after the corrosion test (5000×).

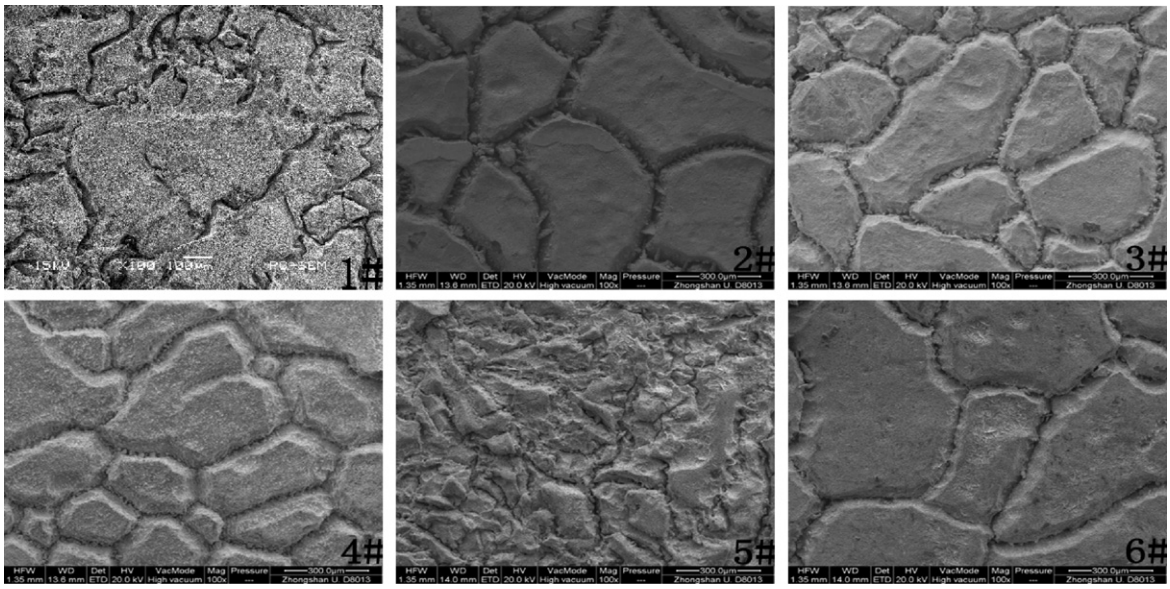

Fig. 14. Morphology of the corroded alloys after removal of the corrosion layers of Pb–Ca–Sn–Al alloys with different La contents after the corrosion test (100×).

2#, 3#, 4#, 5# and 6# alloys electrodes are much clearer and more compact than that on 1# alloy, and there is less production on the surface of the anodic films. The results can be explained that La can easily react with the impurities in the alloy so that deactivate the alloy grain, then clear and increase the density of the anodic film.

3.6. Constant current corrosion test

The morphology of the corrosion layers of the Pb–Ca–Sn–Al alloys with different La contents were observed after corrosion test, and are illustrated in Fig. 13. It can be seen that the corrosion productions of 1# and 5# alloys are composed of irregular-shaped agglomerates, and there are many small need-like crystals embed on the corrosion layer of 1# alloy; while corrosion products of 2#, 3#, 4# and 6# alloys are composed of some dendritic cementation of crystals [20], which can strength the binding force between corrosion layer and active material, and help to prevent the active material peeling, improve corrosion resistance of alloy, reduce premature capacity loss. 3# is the most, 2# the least. Though with the increase of La content, dendritic cementation of crystals of 4# and 6# become to bond into plate-shaped crystals, which may lead to inferior conductivity of anodic film.

The extent of corrosion on lead alloys can be determined by the nature of the surface morphology [8]. As shown in Fig. 14, after removing the corrosion products, the morphologys of the corroded surfaces and the corrosion grain size of 2#, 3#, 4# and 6# alloys are similar. The corrosion extent of 1# and 5# alloys is much heavier than that of 2#, 3#, 4# and 6# alloys, suggesting that the addition of La can deactivate the alloy grain and decrease the corrosion of alloy. The area of grain boundaries is larger because of much finer grain of Pb–Ca–Sn–Al–La alloys, and corrosion occurs preferentially along the grain boundaries, so the grain corrosion of Pb–Ca–Sn–Al–La alloys is lower than Pb–Ca–Sn–Al alloy. The results indicate that proper addition of La can low the grain corrosion, and improve the corrosion resistance of Pb–Ca–Sn–Al alloys, thus prolong the battery life.

4. Conclusions

1. The addition of La can effectively increase the fineness of the grain of Pb–Ca–Sn–Al alloys, especially when the La content is 0.01 wt.%, 0.03 wt.% and 0.1 wt.%.
2. The introduction of La to Pb–Ca–Sn–Al alloys can increase the growth of PbO_2 film, fine and compact anodic film formed at 1.3 V, then increase the conductivity of anodic film. Alloys with 0.01 wt.%, 0.03 wt.% and 0.1 wt.% La were shown satisfactory results.
3. The La additive can decrease the growth of Pb(II) film at 0.9 V, purify and increase the density of the anodic film, then increase the conductivity of passive film, thus reduce premature capacity loss and prolong the cycle-life of lead-acid batteries, especially for the Pb–Ca–Sn–Al alloys with 0.03 wt.% and 0.1 wt.% La.
4. It can be concluded that La can increase the growth of dendritic cementation of crystals, strengthen the binding force between corrosion layer and active material, improve the corrosion resistance of Pb–Ca–Sn–Al alloys, particularly for a La content of 0.01 wt.%.

Acknowledgements

We acknowledge the support of the Guangdong Natural Science Fund Committce; the research fund project is 9151063101000052. The authors would also like to thank Zhuzhou Smelter Group Co. Ltd. in Zhuzhou, Hunan and Zhejiang tianneng Battery Co. Ltd. in Huzhou, Zhejiang for assistance with this project.

References

[1] M. Shiomi, Y. Okada, Y. Tsuboi, S. Osumi, et al., J. Power Sources 113 (2003) 271–276.
[2] K. Sawai, Y. Tsuboi, Y. Okada, et al., J. Power Sources 179 (2008) 799–807.
[3] D. Slavkov, B.S. Haran, B.N. Popov, F. Fleming, J. Power Sources 112 (2002) 199–208.
[4] L.T. Lam, N.P. Haigh, D.A.J. Rand, J. Power Sources 88 (2000) 11–17.
[5] E. Hilali, L. Bouirden, Chim. Ann. J. Sci. Mater. 25 (2000) 91–100.
[6] L. Yang, L. Liu, Y. Pan, et al., J. Power Sources 19 (1995) 15–27.
[7] G. Lin, G. Zhou, D. Li, M. Zheng, J. Rare Earths 24 (2006) 232–237.
[8] A. Li, Y. Cheni, H. Chen, J. Power Sources 189 (2009) 1204–1211.
[9] G. Lin, G. Zhou, D. Li, M. Zheng, J. Rare Earths 23 (2005) 411–414.
[10] W.X. Guo, D. Shu, H.Y. Chen, et al., J. Alloy Compd. 475 (2009) 102–109.
[11] H. Liu, C. Yang, X. Zhang, et al., J. Fudan Univ. (Nat. Sci.) 40 (2001) 688–691.
[12] F. Mansfeld, W.J. Lorenz, in: R. Varma, et al. (Eds.), Techniques for Characterization of Electrodes and Electrochemical Processes, Wiley, New York, 1991, pp. 581–647.
[13] Lasia, in: R.E. White, B.E. Conway, J.O'M. Bockris (Eds.), Modern Aspects of Electrochemistry, vol. 32, Kluwer Academic/Plenum Press, New York, 1999, pp. 143–248.

[14] G. Inzelt, G. Lang, J. Electroanal. Chem. 378 (1994) 39–49.
[15] J. Benavente, J.R. Ramos-Barrado, A. Cabeza, J. Colloid Interface Sci. 180 (1996) 116–121.
[16] T.M. Nahir, E.F. Bowden, Electrochim. Acta 39 (1994) 2347–2352.
[17] R.P. Janek, W.R. Fawcett, A. Ulman, J. Phys. Chem. B 101 (1997) 8550–8558.
[18] L.V. Protsailo, W.R. Fawcett, Electrochim. Acta 45 (2000) 3497–3505.
[19] D. Li, G. Zhou, G. Lin, M. Zheng, J. Rare Earths 23 (2005) 353–357.
[20] C.S. Lakshmi, J.E. Manders, D.M. Rice, J. Power Sources 73 (1998) 23–29.